MERGING OF VARIABLE-RESOLUTION IMAGERY USING GEOSTATISTICS AND SENSOR PSFS

Tyler Erickson, Ph.D., Senior Analyst
Altarum Institute
Ann Arbor, MI 48105
tyler.erickson@altarum.org

Anna M. Michalak, Ph.D., Assistant Professor
Department of Civil and Environmental Engineering, and
Department of Atmospheric, Oceanic and Space Sciences
University of Michigan
Ann Arbor, MI 48109-2125
anna.michalak@umich.edu

ABSTRACT

Current remote sensing analysis methods typically treat imagery as a regular grid of rectangular pixels representing regions with uniform information. In reality, a pixel represents a non-uniform integration of spatial information described by the sensor's point spread function (PSF). This conceptual simplification of the sensor's support facilitates the presentation of single images, but often prevents statistically rigorous analyses of imagery. This paper presents a methodology for merging multiple (source) images from sensors with dissimilar PSFs into a new (target) image, using a geostatistical inverse modeling framework. The inverse model takes into account the sensor PSFs, the spatial correlation of the information being modeled, and the measurement error of the source images. The inverse model yields both a best estimate of the target image and the estimation (co)variance of the target data. The inverse model approach is quite general and can be used to address many issues in remote sensing image analysis such as upscaling or downscaling imagery to different spatial supports, or merging variable-resolution images with different grid orientations. The methodology is can be applied to irregularly spaced data (such as images with geometric distortion due to rugged topography) or images with missing values (such as partially cloud-obscured optical images).

INTRODUCTION

Current remote sensing analysis methods typically treat electro-optical imagery as a regular grid of rectangular pixels with uniform information, where in reality a pixel represents a non-uniform integration of spatial support described by the sensor's point spread function (PSF). The difference between an idealized PSF and a realistic model of an actual sensor PSF is illustrated in Figures 1 and 2. Figure 1 illustrates an idealized PSF of a sensor that is uniformly sensitive to signal within a rectangular region, corresponding to the boundaries of a remote sensing image pixel. Figure 2 illustrates a realistic PSF of a sensor modeled by a two-dimensional Gaussian distribution (Townshend, 2000).

This conceptual simplification of a sensor's response facilitates the presentation of images of remote sensing data, but hinders statistically rigorous analyses of the sensor data. A sensor's PSF causes measurement values to be a weighted average of the signal both inside and outside of the pixel boundary. For example, approximately 50% of the signal for a pixel in a MODIS image originates from outside the pixel boundary (Townshend, 2000).

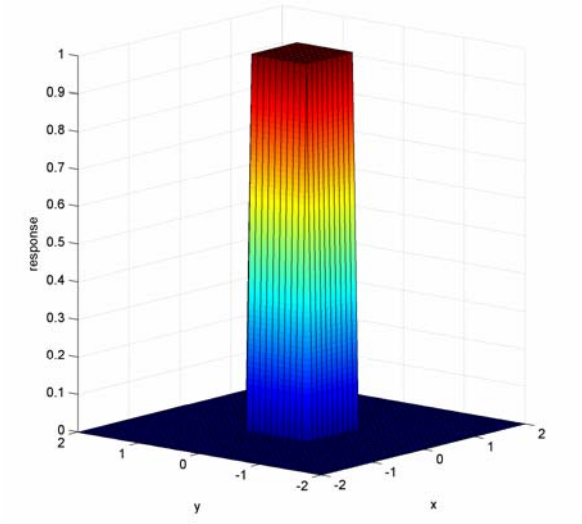

Figure 1. An idealized PSF which uniformly weights the sensor signal within the boundaries of a rectangular area corresponding to the pixel boundaries.

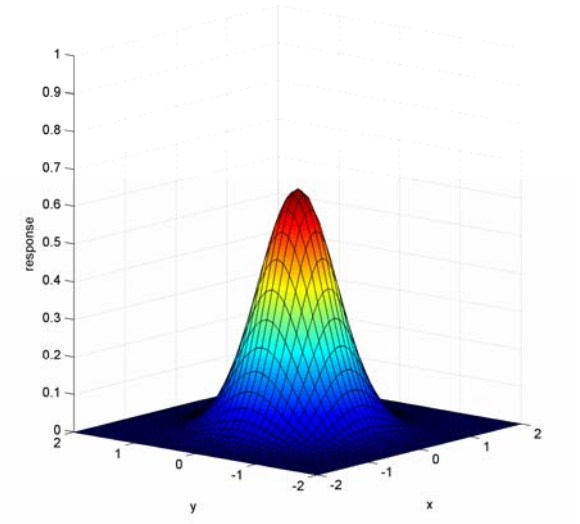

Figure 2. A two-dimensional Gaussian PSF. The Gaussian PSF models the non-uniform sensitivity of a measurement to signal from both inside and outside the pixel boundary.

This paper presents a methodology of incorporating a realistic model of the sensor's PSF to improve estimates of the surface properties being observed. The methodology can be applied to a single remote sensing dataset, or can be used to merge multiple (source) datasets from sensors with dissimilar PSFs into a new (target) image. The methodology is based on the geostatistical inverse modeling framework. The inverse model takes into account the sensor PSFs, the spatial correlation of the information being modeled, and errors of the source measurements. The inverse model yields both a best estimate of data in the target image and the estimation (co)variance of the target data points. An overview of the geostatistical inverse model methodology is shown in Figure 3. The methodology, inputs, and outputs are further described in the following sections.

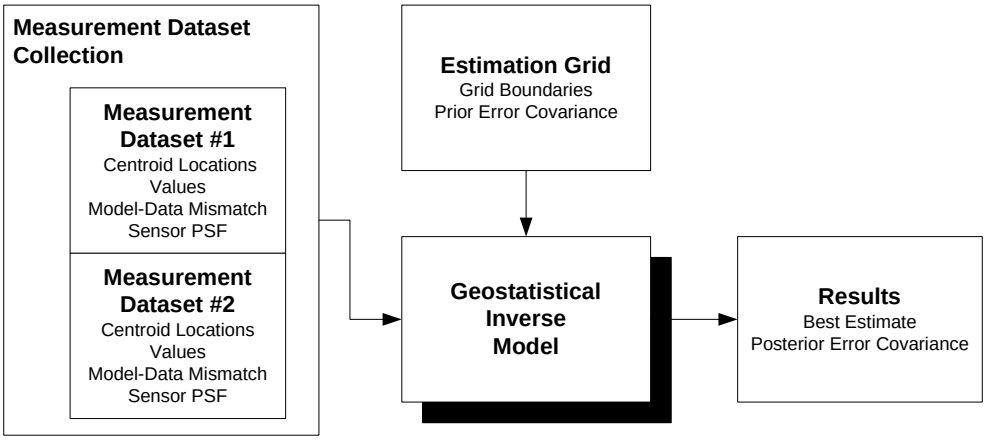

Figure 3. Overview of the geostatistical inverse model methodology for remote sensing images. One or more remote sensing measurement datasets with model-data mismatch errors and PSF models are fed into the geostatistical inverse model. For the locations specified in the estimation grid, the model produces both best estimates and a measure of the uncertainty (posterior error covariance).

METHODOLOGY

General Setup

The standard estimation problem is to estimate the surface properties from remote sensing data with finite support, which we will formulate as a geostatistical inverse problem. Only the key equations are presented, and the reader is referred to Michalak et al. (2004) for a more in-depth discussion of the geostatistical methodology.

The estimation problem may be expressed as:

$$\mathbf{z} = h(\mathbf{s}, \mathbf{r}) + \boldsymbol{\upsilon}$$

where $\mathbf{z}$ is an $n \times 1$ vector of observations obtained by remote sensing and $\mathbf{s}$ is an $m \times 1$ state vector obtained from the discretization of the surface properties that we wish to estimate. The vector $\mathbf{r}$ contains other parameters needed by the transformation model function $h(\mathbf{s},\mathbf{r})$. The model-data mismatch (error) is represented by the vector $\boldsymbol{\upsilon}$. This error encompasses both the measurement error associated with collecting the data and any random numerical or conceptual inaccuracies associated with the evaluation of the function $h(\mathbf{s},\mathbf{r})$. When the function $h(\mathbf{s},\mathbf{r})$ is linear with respect to the unknown $\mathbf{s}$, it can be written as:

$$h(\mathbf{s}, \mathbf{r}) = \mathbf{H}\mathbf{s}$$

where $\mathbf{H}$ is a known $n \times m$ matrix, the Jacobian representing the sensitivity of the observations $\mathbf{z}$ to the surface properties $\mathbf{s}$ (i.e. $H_{ij} = z_i / s_j$ where i is the index of observations and j is the index of estimation locations). The sensitivity matrix is calculated in the same way whether one or multiple measurement datasets are considered. In the case of multiple measurement datasets, the sensitivity matrix can be partitioned into

$$\mathbf{H} = \begin{bmatrix} \mathbf{H}_1 \\ \vdots \\ \mathbf{H}_G \end{bmatrix}$$

where G is the number of measurement datasets.

The state vector is modeled as a random function with a constant (unknown) mean

$$E\{\mathbf{s}\} = \mathbf{X}\boldsymbol{\beta}$$

where E[ ] is the expectation operator, $\mathbf{X}$ is a known $m \times 1$ matrix of ones, and $\boldsymbol{\beta}$ is the unknown mean of the random function.

The prior covariance matrix is used to describe the spatial correlation of the state values

$$\mathbf{Q} = E\left[(\mathbf{s} - \mathbf{X}\boldsymbol{\beta})(\mathbf{s} - \mathbf{X}\boldsymbol{\beta})^T \right]$$

The best estimate and posterior variance of the surface properties are found by solving the following system of linear equations

$$\begin{bmatrix} \mathbf{HQH}^T + \mathbf{R} & \mathbf{HX} \\ \mathbf{X}^T & \mathbf{0} \end{bmatrix} \begin{bmatrix} \boldsymbol{\lambda}^T \\ \mathbf{M} \end{bmatrix} = \begin{bmatrix} \mathbf{HQ} \\ \mathbf{X}^T \end{bmatrix}$$

where **R** is model-data mismatch. The best estimate of the surface properties is given by

$$\hat{\mathbf{s}} = \boldsymbol{\lambda}^T \mathbf{z}$$

and the posterior covariance matrix of the surface properties is

$$\mathbf{V}_{\hat{s}} = \mathbf{XM} + \mathbf{Q} - \mathbf{QH}^T \boldsymbol{\lambda}^T$$

The diagonal elements of the posterior covariance matrix represent the posterior variances of the properties at the individual surface locations. The square root of the posterior variance is the standard error of estimation.

MODEL SELECTION

Sensor Point Spread Functions (PSFs)

The sensitivity of the observations to the surface properties is primarily controlled by the sensor's optics, although other factors such as viewing geometry and atmospheric effects may be significant. The sensor's optics are generally described by a PSF), which describes the response of a single image pixel to the surface properties under ideal conditions. An appropriate model of the PSF for many electro-optical sensors is the two-dimensional symmetrical Gaussian distribution (Huang et al., 2002)

$$H_{i,j} = PSF(x_i, s_j) = \exp\left(\frac{-(x - u)^2 - (y - v)^2}{2\sigma_{psf}^2} \right)$$

where x and y are the coordinates of estimate locations in the image space, u and v are the local coordinates relative the center of the measurement, and σ_{psf} is the scaling factor which describes the spread of the PSF. The scaling factor and pixel spacing are generally related, with the pixel spacing being approximately double the scaling factor. For example, MODIS 250-m bands can be modeled with a scaling factor of 123.5 m (Barker and Burelhach, 1992).

Covariance Model

The prior covariance matrix is used to describe the expected spatial correlation of the surface properties. We model this using an exponential covariance function:

$$Q_{ij} = \sigma_{sill}^2 \exp\left(\frac{-h_{ij}}{l} \right)$$

where σ^2_{sill} is the sill semi-variance, h_{ij} is the separation distance between surface property locations and $\boldsymbol{l}$ is the integral scale (which is approximately a third of the effective correlation range).

The measurement error covariance matrix is used to model the expected covariance of the model-data mismatch. For this work, we will assume all measurement errors are independent and have a uniform variance. Under these assumptions, the measurement error covariance matrix is modeled as

$$\mathbf{R} = \sigma^2_R \mathbf{I}$$

where σ^2_R is the variance of the measurement error, and $\mathbf{I}$ is an $n \times n$ identity matrix.

SAMPLE APPLICATION

The following section presents a sample application of merging two remote sensing datasets of differing resolutions, grid orientations, and spatial extent. The two datasets were derived from a source image of finer resolution, which will be considered to be the 'truth,' and to which the measurement datasets and inversion estimates will be compared.

Source Image

The source image (Figure 4) is a 100 by 100 pixel true-color image of the Boston harbor area, corresponding to a 400 by 400 m ground extent. To illustrate the method, the red band of the image was extracted and colored according to its digital number (DN), which ranges from 0 to 255 (Figure 5). Several features can be identified within the image, such as a bridge and its shadow, two lanes extending over the waterfront, and several watercrafts.

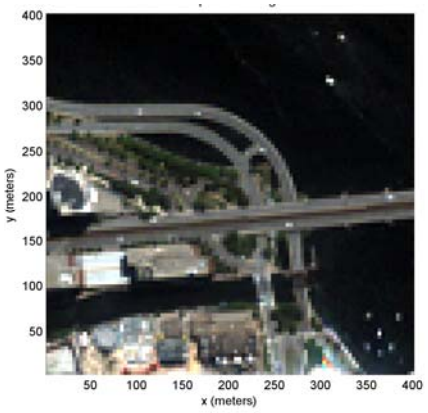

Figure 4. The RGB source image of a waterfront area, with a total extent of 400 by 400 meters. (Image copyright Space Imaging LLC)

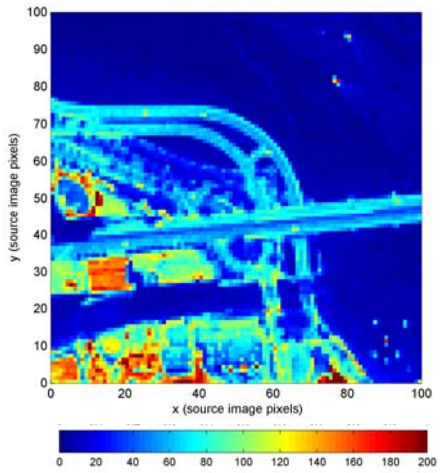

Figure 5. The red channel of the source image used to generate the measurement datasets. The reflectance is specified in units of digital numbers (DN).

Simulation of Measurements

Two datasets were simulated from the source image using the PSF model. Dataset #1 is a 20 by 20 grid at a 5 pixel spacing, and uses a PSF scaling factor of 2.5 pixels. From a map of these measurements (Figure 6a), the difference between water and land is evident, and the prominent linear features of the bridge and its shadow can be identified, but it is difficult to identify small features present in the source image.

Dataset #2 is a 40 by 10 grid at a 2.5 pixel spacing, and uses a PSF scaling factor of 1.25 pixels. This dataset of

measurements only covers 25% of the area of the source image. Within the extent of this dataset (Figure 6d), additional features can be identified, such as the separate road lanes extending over the waterfront.

Inverse Model Results

From the measurement datasets, we seek to obtain a best estimate and standard error for each cell in a 50 by 50 grid covering the entire extent of the source image. Each grid cell covers the area of 2 by 2 pixels of the source image. We assumed reasonable values to parameterize the inverse model components, but did not optimize the parameters to the datasets. The variance of the measurement error was assumed to be $2\ DN^2$ for all measurements, while a sill variance of σ^2_{sill}=10 DN^2 and an integral length of l=2 pixel units were used for the exponential covariance model of the surface properties.

The results of the geostatistical inverse model based on the sensor datasets are shown in Figure 6. The first column of images displays the location and values of the sensor measurements, the second column presents the best estimate produced by the geostatistical inverse model, and the third column presents the estimation standard error produced by the geostatistical inverse model. The estimation standard error image quantifies the uncertainty of the estimate for each grid cell of the estimation image, and is controlled by the relative locations of the measurements and grid estimation cells, as well as other model parameters. Cool colors (blue) indicate relatively low uncertainty of the estimated value, while warm colors (red) indicate relatively high uncertainty. The first row contains the images for Dataset #1 (coarse resolution, full extent), the second row contains the measurements and results of Dataset #2 (fine resolution, limited extent), and the third row contains the measurements and results when both Dataset #1 and Dataset #2 are considered simultaneously.

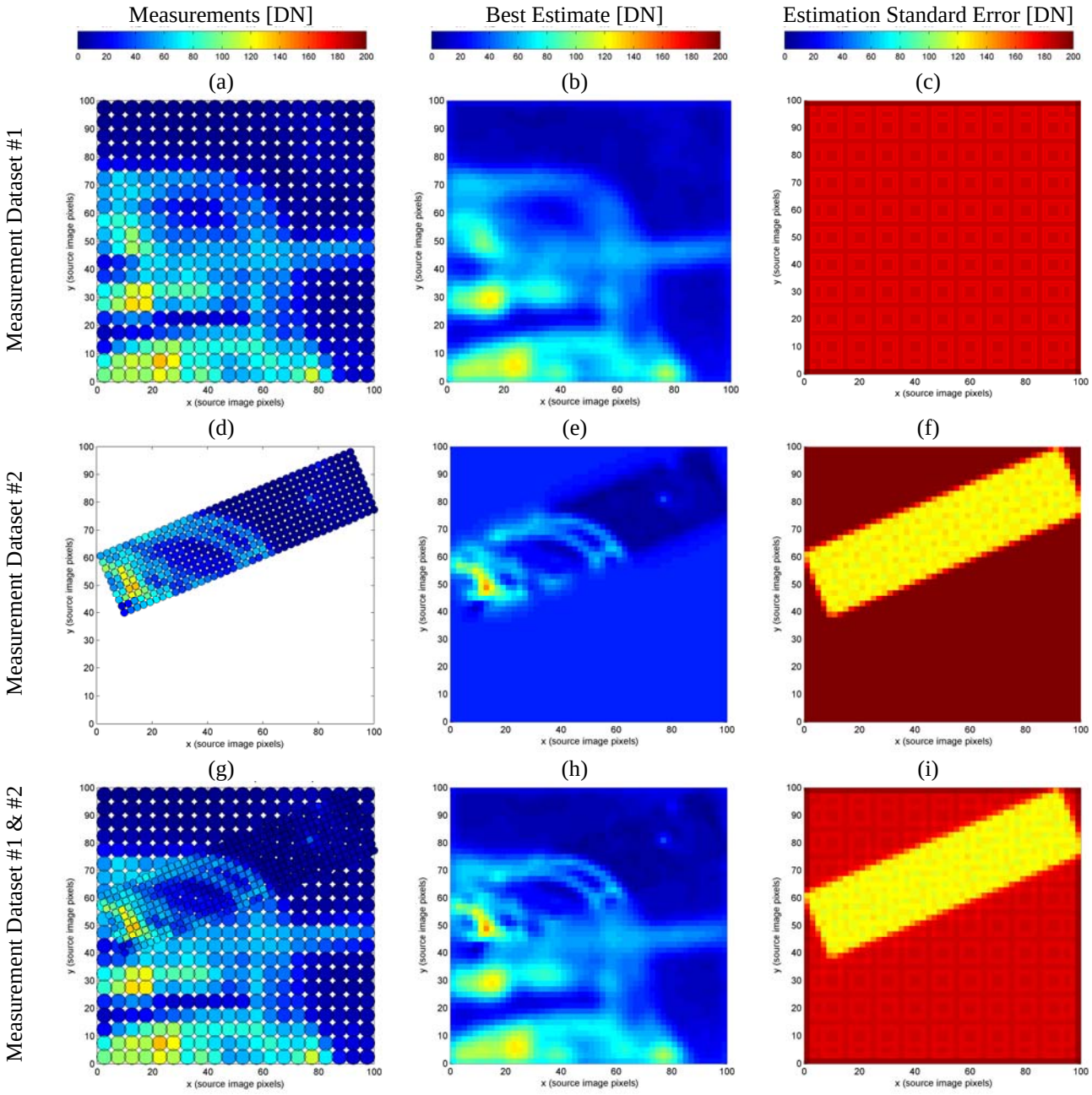

Figure 6. Images of the sensor measurements, inverse model best estimates, and estimation standard errors for measurement Dataset #1, Dataset #2, and both datasets simultaneously. The axis units are in pixels of the source image (Figure 5).

The benefit of incorporating a realistic PSF of the sensor is illustrated by comparing the sensor measurement image (Figure 6a) to the best estimate image (Figure 6b) for Dataset #1. The best estimate image is more detailed because the inverse model deconvolves the spreading effect of the sensor, and is therefore able to reproduce more of the contrast and the high and low values of the source image (Figure 5). The estimation standard error values (Figure 6c) are influenced by the distance between the PSF centroid and the estimation grid, and the image appears as a regular pattern due to the alignment of the measurement and estimation grids. The estimation standard error image is relatively uniform, due to the uniform distribution of the measurements.

The results for Dataset #2 illustrate how a relatively high resolution dataset can improve the results of the inverse

model. Within the extent of the measurements (Figure 6d), the best estimate (Figure 6e) displays higher contrast and more features (relative to Figure 6b) of the original source image (Figure 5). Outside the extent of the high-resolution measurements, the best estimate is uniform. The estimation standard error (Figure 6f) illustrates that the uncertainty is relatively low in the vicinity of the high-resolution measurements, and is uniformly high outside the extent of the measurements.

The third row of Figure 6 illustrates the results when both the low-resolution (Dataset #1) and high-resolution (Dataset #2) datasets are merged within the geostatistical inverse model. Figure 6g shows the relative placement of the two datasets. Within the extent of the high-resolution measurements, the best estimate image (Figure 6h) exhibits relatively high contrast and the estimation uncertainty is low (Figure 6i), relative to the area where only low-resolution measurements are available.

DISCUSSION

The sample application presented in this paper demonstrates the ability of geostatistical inverse modeling to 1) recover the source image by taking into account the sensor's PSF, and 2) combine information from two remote sensing images with different pixel resolutions, grid orientations, and geographic extents. The presented methodology could also be used to merge information from more than two datasets, such as merging the four or more daily MODIS images obtained from the ascending and descending paths of the NASA's AQUA and TERRA satellites.

The sample application also demonstrates the methodology's ability to produce estimates at a finer resolution than that of the measurements. Similarly, by choosing a coarse estimation grid, the methodology could be used to produce estimates on an upscaled resolution grid (larger grid cells). The methodology could be applied to multiple bands of a image, and bands could be assumed to be independent or correlation between bands could be modeled.

The methodology could be applied to a collection of images to limit or remove the effect of clouds, by merging datasets with differing cloud cover. Cloud-affected measurements could be incorporated by one of two methods. The first method would be to remove cloud-obscured measurements from the vector of observations ($\mathbf{z}$), so that these measurements would not be considered in the inversion. The second method would be to prescribe a higher model-data mismatch error ($\boldsymbol{v}$) variance for cloud-affected measurements, such that this measurement information would be included but would be treated as less precise than the cloud-free measurements.

The methodology does not require the measurements to be aligned in a regular grid. For example, the presented approach could be used to produce orthogonally gridded products from the Landsat 7 Enhanced Thematic Mapper Plus sensor, which suffered the loss of the scan line corrector mechanism resulting in a zig-zag pattern across the satellite ground track. This could either be performed on a single Landsat scene, or could be performed on a series of Landsat images to reduce the estimation uncertainty in the 'gap' regions of the zig-zag pattern.

The presented sample application uses a two-dimensional Gaussian function to model the PSF of electro-optical sensors. More realistic models could be easily incorporated, such as models that incorporate the sensor optics, detector, filters, atmospheric transmission, and motion blur. Improvements in the PSF would decrease the model-data mismatch, and thereby lower the estimation variance.

By relaxing some of the assumptions utilized in the present description, the methodology could be extended to apply to other issues related to merging datasets. Currently, the sensitivity matrix is only based on the sensor PSF model and assumes a nadir looking sensor, viewing flat terrain. The sensitivity matrix could be adapted to take into account the changes in the geometric field of view when viewing areas of rugged topography. This adaptation would be particularly useful when integrating multiple non-nadir looking sensors, because the dissimilar measurement footprints would provide additional information to the inverse model.

Finally, the current methodology was presented assuming a constant (unknown) mean. This assumption could be relaxed to allow for a piecewise or smoothly varying mean, which could be used to incorporate additional information known about the estimated properties, such as land cover information. Incorporating additional information into the mean model has been demonstrated to produce improved estimates in geostatistical interpolation (Erickson et al., 2005) as well as geostatistical inverse modeling (Michalak et al., 2004 and 2005ab; Mueller et al., 2005; Gourdji et al., 2005).

CONCLUSIONS

A methodology for integrating the information contained in multiple remote sensing images was described. A sample application was presented which integrated two datasets with different measurement spacings, grid orientations, and spatial extents. The methodology is quite flexible, and can be extended to address current issues in electro-optical remote sensing such as upscaling/downscaling of images at varying resolutions, cloud removal, and integration of off-nadir viewing sensors.

REFERENCES

Barker, J. L. and J. W. Burelhach (1992). MODIS image simulation from Landsat TM imagery. In: *ASPRS/ACSM/RT 92*. Bethesda, Washington, DC, American Society for Photogrammetry and Remote Sensing: 156-165.

Erickson, T. A., M. W. Williams, and A. Winstral (2005). Persistence of topographic controls on the spatial distribution of snow in rugged mountain terrain, Colorado, USA. *Water Resources Research*, 41(W04014), doi:10.1029/2003WR002973.

Gourdji, S., K. Mueller, C. Humphriss, and A. M. Michalak (2005). Fine spatial resolution global CO2 flux estimates for 1997 to 2001 obtained using remote-sensing derived environmental data within a geostatistical inverse model. *Eos Transactions AGU, Fall Meeting Supplement* 86(52):Abstract A13G-03.

Huang, C., J. R. G. Townshend, S. Liang, S. N. V. Kalluri, and R. S. DeFries (2002). Impact of sensor's point spread function on land cover characterization: assessment and deconvolution, *Remote Sensing of Environment*, 80:203-212.

Michalak, A. M., A. Hirsch, L. Bruhwiler, K. R. Gurney, W. Peters, and P. P. Tans (2005). Maximum likelihood estimation of covariance parameters for Bayesian atmospheric trace gas surface flux inversions. *Journal of Geophysical Research* 110(D24), doi:10.1029/2005JD005970.

Michalak, A. M., K. Mueller, S. Gourdji, C. Humphriss, L. Bruhwiler, K. Schaefer, and P. P. Tans (2005). Application of a geostatistical kalman smoother to the estimation of monthly gridscale fluxes of carbon dioxide. Pages p.301-302 In: *7th International Carbon Dioxide Conference*, Boulder, Colorado.

Michalak, A. M., L. Bruhwiler, and P. P. Tans (2004). A geostatistical approach to surface flux estimation of atmospheric trace gases, *Journal of Geophysical Research*, 109(D14109), doi:10.1029/2003JD004422.

Mueller, K., S. Gourdji, K. Shaefer, C. Humphriss, and A. M. Michalak (2005). Using remote sensing data to help constrain fluxes of CO2 in a geostatistical inverse modeling framework. In: *Eos Transactions AGU, Fall Meeting Supplement* 86(52):Abstract A13G-02.

Townshend, J. R. G., C. Huang, et al. (2000). Beware of per-pixel characterization of land cover. *International Journal of Remote Sensing*, 21(4): 839-843.